IOP Publishing Nanotechnology

Nanotechnology **27** (2016) 085605 (10pp) doi:10.1088/0957-4484/27/8/085605

Controllable *in situ* photo-assisted chemical deposition of CdSe quantum dots on ZnO/CdS nanorod arrays and its photovoltaic application

Xinwei Wang, Hong Liu and Wenzhong Shen

Laboratory of Condensed Matter Spectroscopy and Opto-Electronic Physics, Key Laboratory of Artificial Structures and Quantum Control (Ministry of Education), Institute of Solar Energy, Department of Physics and Astronomy, Shanghai Jiao Tong University, 800 Dong Chuan Road, Shanghai, 200240, People's Republic of China

E-mail: liuhong@sjtu.edu.cn and wzshen@sjtu.edu.cn

Received 8 October 2015, revised 8 December 2015
Accepted for publication 21 December 2015
Published 28 January 2016

Abstract

Compound semiconductors have been widely applied in the energy field as light-harvesting materials, conducting substrates and other functional parts. Nevertheless, to effectively grow them in various forms toward objective applications, limitations have often been met to achieving high growth rate, simplicity of method and controllability of growing processes simultaneously. In this work, we have grown a uniform CdSe layer on ZnO/CdS nanorod arrays by a novel *in situ* photo-assisted chemical deposition method. The morphology and quality of the as-formed material could be significantly influenced by tuning the optical parameters of the injected light. Due to the effect of injected light on the key reactions during the growth, a modified natural light with removal of the UV and IR components seems to be more suitable than monochromic light. An efficiency of 3.59% was achieved without any additional treatment, significantly higher than the efficiency of 2.88% of the sample by conventional CBD method under similar conditions with growth rate one order of magnitude higher. In general, the result has suggested its potential importance for other compound materials and opto-electronic devices.

S Online supplementary data available from stacks.iop.org/NANO/27/085605/mmedia

Keywords: targeting growth, photochemical deposition, quantum dots and thin films, nanorods, photoelectrochemical solar cells

(Some figures may appear in colour only in the online journal)

1. Introduction

With the ever-increasing demand for clean energy, tremendous effort has been paid to developing high performance solar cells by simple and controllable methods [1–4]. For instance, photoelectrochemical cells (PECs) have shown their own advantages of low cost, environmentally friendly fabrication and easily tunable electronic and optical properties [5–9]. In a typical PEC, dye particles or quantum dots (QDs) have often functioned as the light absorbers and played an important role together with various carrier transporters of nanostructured semiconductor substrates [10–13]. Compound semiconductors such as CdS [14], PbS [15], CdSe [16–18] and CdTe [19] have shown promising properties for the QD materials due to their simplicity for fabrication and easily tunable electronic and optical properties, while ZnO has been a focused candidate for the substrate due to adequate electron mobility (196 $\mathrm{cm^2\,V^{-1}\,s^{-1}}$, wurtzite) [20] and easily modifiable morphology [21, 22]. With co-sensitization of CdSe and CdS QDs, ZnO nanostructure-based PECs have yielded an efficiency of around 3–5% [23–26].

However, the efficiency of ZnO supported sensitized solar cells has been often negatively influenced by its relatively low adsorption ability of particles compared with other oxide surfaces. Moreover, the fabrication of solar cells based on compound semiconductors is still normally a long or complicated process, which is also true of systems based on other substrates. Conventional fabrication methods normally follow two strategies: *ex situ* and *in situ*. The first strategy is to fabricate the compounds by hydrothermal or photochemical reactions, distribute the products in colloids and then install them into targeted substrates via direct or linker-assisted adsorption [27–30]. These *ex situ* methods can ensure good QD quality but with the expense of more complicated procedures and low loading efficiency of particles into targeted substrates, i.e., ZnO nanostructures. The second is to directly grow QDs onto substrates through the chemical bath deposition (CBD) [31, 32], successive ionic-layer adsorption and reaction (SILAR) [33], electrochemical deposition (ECD) [34], photochemical deposition (PCD) [35–38] and chemical vapor deposition (CVD) [39]. These methods can achieve satisfying growth rates and good combination of QDs to the substrates, which are important to applicable high performance solar cells and other devices. However, the complexity of fabrication (SILAR, ECD) and high cost of fabrication method (CVD) have significantly inhibited their applications. The CBD method, though it has simpler procedures, has often been limited by the reaction conditions such as precursor selection, high reactor concentration and suitable pH value or ambient temperature [26, 40], which have also lowered the stability and controllability of the reaction toward purposed opto-electronic properties. The PCD method has shown its own comparative simplicity and efficiency [3, 35, 41–43]. However, the type of materials are quite limited since most of the systems are single precursor systems, and difficulty also remains in developing materials into nanostructured substrates (nanorods, nanotubes, nanoflowers, etc) with effective control of the growth via detailed parameters of the applied light. Therefore, a combination with the advantages of these methods can hopefully resolve the problem.

In this work, we have developed a novel photo-assisted chemical deposition (PACD) through reactions of a few precursors under excitation of controllable light sources, which can fabricate uniform CdSe material on ZnO/CdS nanorod arrays with a high growth rate at room temperature. Corresponding sensitized solar cells based on them have achieved a conversion efficiency of 3.59% without chemical decoration, significantly higher than that of the control sample (2.88%) by normal CBD method with growth time much shorter (1.5 h versus 16 h). Moreover, the morphology and dimension of the as-formed structure can be effectively influenced when tuning the external light source. These phenomena have suggested the role of photon-excitation of carriers from the substrate and thus influenced the main reaction steps in the CdSe formation. The experiment of time series also indicated a top-down growth of CdSe on ZnO/CdS in this method. In general, the results have shown an effective and controllable way to grow compound semiconductors on nanostructure substrates simply by an external light field and can hopefully be applied to various other systems.

2. Methods

2.1. Fabrication of ZnO/CdS nanorod arrays

ZnO nanorod arrays were prepared by a two-step method on FTO glass. In the first step, FTO glass was immersed in a 5.0 mM zinc acetate ($Zn(CH_3COO)_2$) ethanol solution for 10 s and then dried by nitrogen flow. This process was repeated five times. The substrates were heated in air at 350 °C for 20 min. In the second step, the samples were vertically installed onto a rubber holder and immersed in Teflon-lined stainless-steel autoclaves (with 25.0 mM zinc nitrate ($Zn(NO_3)_2$) and 25.0 mM hexamethylenetetramine) kept at 92 °C for 6 h and repeated for 6 times. After the reaction, the sample was cleaned in deionized water and annealed in air at 450 °C for 30 min. To fabricate the ZnO/CdS substrate, the as-prepared substrates were immersed into a 20 ml solution of 0.1 M sodium sulfide (Na_2S) for 10 min at room temperature. Subsequently, the samples were immersed in a solution mixed of 0.025 M cadmium acetate ($Cd(CH_3COO)_2$), 0.1 M thiourea and 0.1 M ethylenediamine and kept at room temperature for 1 h [44].

2.2. Fabrication of CdSe layer on ZnO/CdS substrates

In the control experiment using the CBD method, a 30 ml aqueous solution was prepared by mixing 0.1 M $Cd(CH_3OO)_2$, 0.1 M Na_2SeSO_3 aqueous and 0.2 M $N(CH_2COONa)_3$ with volume ratio 1:1:1. Afterwards, the previously fabricated ZnO/CdS substrates were vertically immersed in the solution and kept at room temperature for 9 to 24 h under dark condition. For the visible laser PACD deposition of CdSe layer, the illumination was introduced into the same mixed solution by adding semiconductor laser devices with a power of 50 mW and wavelength $\lambda = 405$, 450, 532, 650 and 780 nm. The power density of the laser was controlled by tuning the beam diameter to 28, 22, 15, 10 and 8 mm by a lens system. For PACD experiment on mixed wavelengths, two light sources were applied: a standard AM 1.5 solar simulator (Oriel sol-2A, Newport) equipped with a UV/IR blocker filter ($400\ \text{nm} < \lambda < 720\ \text{nm}$) and a 175 W high pressure mercury lamp.

2.3. Fabrication of PEC solar cells

After the deposition of CdSe layer, the as-prepared samples were coated with ZnS by twice dipping alternately into 0.1 M $Zn(CH_3COO)_2$ and 0.1 M Na_2S aqueous solution for 1 min per dip. They were then annealed at 300 °C in argon atmosphere for 5 min and used as the photoanode of the PEC solar cells. The Cu_2S counter electrode was fabricated by immersing brass in a 37% HCl solution at 70 °C for 5 min and then vulcanized with as-prepared polysulfide electrolyte (composed of 2.0 M Na_2S, 2.0 M S, and 0.2 M KCl in 30 vol.% methanol aqueous solution). The photoanode and counter electrode were mounted together with a 50 μm spacer with a dip (10 μl) of polysulfide electrolyte.

2.4. Characterization of the materials and devices

The morphology of the samples was mainly characterized by scanning electron microscopy (FE-SEM Sirion 200, JEOL JSM). The elemental analysis was performed by energy dispersive x-ray (EDX) during the SEM observation. More detailed morphology and the microstructure were investigated by a high resolution transmission electron microscopy (JEM-2100F, JEOL USA Inc.). The crystal structure and chemical composition of the samples were further characterized by x-ray diffraction (XRD, D/max-2200/PC) with high intensity Cu Kα radiation (1.5406 Å) and room-temperature Raman spectroscopy (HR 800UV micro-Raman/PL system, Jobin Yvon LabRAM) at 514.5 nm. The absorption spectra were recorded with a lambda-750 UV/vis/NIR spectrophotometer. The current density–voltage (*J–V*) characteristics of the solar cells were measured by computer programmed Keithley 2400 sourcemeter under AM 1.5 (100 mW cm^{-2}) illumination provided by solar simulator (Oriel sol-2A, Newport). The external quantum efficiency (EQE) was measured by a quantum efficiency measuring system (QEX 10, PV Measurements).

3. Results

3.1. CdSe growth on ZnO/CdS substrate by conventional CBD method

For comparison, CdSe was also grown by the conventional CBD method on ZnO/CdS nanorods. As the substrate, the ZnO/CdS core–shell nanorods were prepared by the typical CBD process to deposit a CdS layer on the ZnO nanorods using $Cd(CH_3COO)_2$, thiourea and ethylenediamine as precursors [44]. As shown in figure 1(a), the as-fabricated nanorods have an average diameter of about 170 nm. Afterwards, the sample was immersed in a mixed solution of cadmium acetate, sodium selenosulphate and trisodium salt of nitrilotriacetic acid and kept at room temperature for 16 h. After the reaction, the average diameter of the nanorods increased to about 190 nm (figure 1(b)). TEM images in figure 1(c) demonstrate that nanocrystal grains were formed on the nanorod surface with the size of 3–10 nm. The inset has shown the spacing of about 0.35 nm between the atomic layers, consistent with (111) plane of CdSe. The XRD diffraction peaks at 26.8° in spectrum I in figure 1(d) corresponds to the cubic (111) plane (JCPDS no. 21-0829) of CdS, while the one at 25.4° in spectrum II is related to (111) plane of CdSe (JCPDS no. 65-2891). The Raman spectra I and II in figure 1(e) are corresponding to the sample before and after the deposition, respectively. The peak at 300.8 cm^{-1} in spectrum I corresponds to the first-order longitudinal optical phonon modes (1LO) of CdS [45]. The peaks at 204.2 cm^{-1} and 298.1 cm^{-1} in spectrum II are assigned to the 1LO mode of CdSe [46] and CdS, respectively. The small downshift of the CdS 1LO mode may be induced by the mismatch and tension in the interface of the core–shell structure [47]. Furthermore, UV/vis/NIR was performed to characterize the optical absorption properties of the control samples. As presented in figure 1(f), strong absorption took place when $\lambda < 520$ nm for ZnO/CdS nanorods. After the deposition of the CdSe layer, the absorption edge shifted up to ~680 nm, showing significant enhancement of the light absorption.

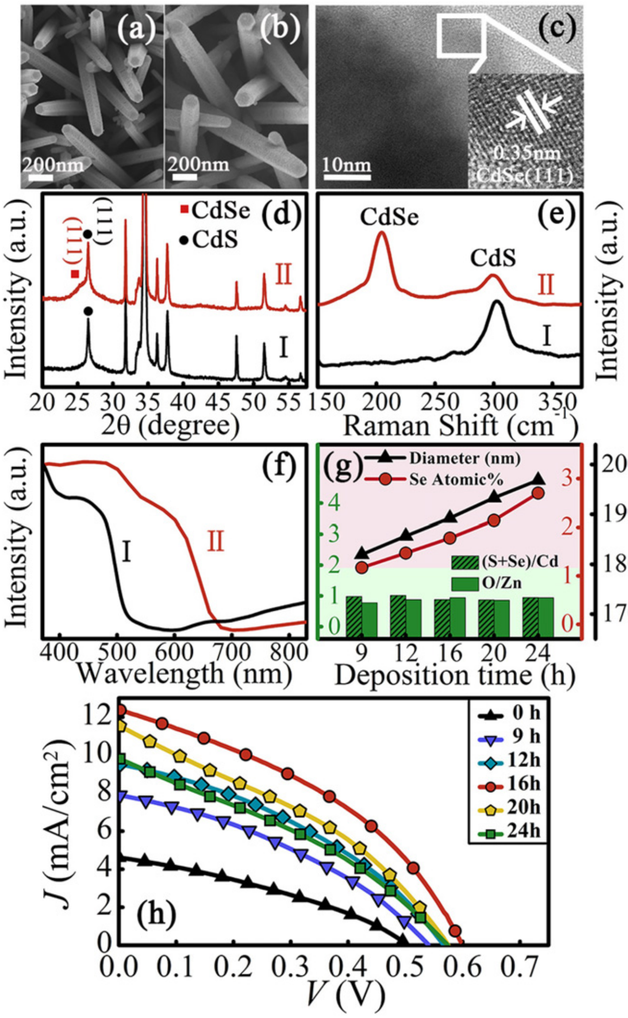

Figure 1. CBD CdSe layer on ZnO/CdS nanorods substrates and the corresponding cell performance: (a),(b) top-view SEM images of sample: (a) before and (b) after CBD deposition for 16 h, respectively; (c) TEM image of ZnO/CdS/CdSe nanorod; (d) XRD of the sample before (I) and after (II) deposition; (e) Raman spectroscopy of the sample before (I) and after (II) deposition; (f) diffused reflectance spectra of the sample before (I) and after (II) deposition; (g) average diameter, Se content, ratio of atomic content (O/Zn, (S + Se)/Cd) versus different deposition time, measured by EDX; (h) *J–V* characteristics of PEC solar cells with different deposition time.

Moreover, the deposition time was varied from 9 to 24 h to optimize the products. Figure 1(g) indicates that the content of Se and the diameter of nanorods monotonically increased with longer growth time from 1.17% to 2.70% and from 180 to 200 nm, respectively, while the ratio of the contents (Se + S)/Cd and O/Cd remained stable. Subsequently, the samples were integrated into sandwich-type PEC solar cells, with their photocurrent density–voltage (*J*–*V*) characteristics shown in figure 1(h). Before deposition, the ZnO/CdS nanorods alone showed a conversion efficiency of 0.99% in PEC cells, with $J_{SC} = 4.62$ mA cm^{-2}, $V_{OC} = 0.506$ V, and FF = 0.35. After deposition of CdSe, the cell performance was significantly increased. The conversion efficiency increased as the deposition time increased from 9 h to 16 h and then decreased as the deposition time increased from 16 h to 24 h. Eventually, the cell efficiency achieved a maximum value of 2.88% with $J_{SC} = 12.37$ mA cm^{-2}, $V_{OC} = 0.597$ V, and FF = 0.39, with the deposition time of 16 h.

3.2. CdSe formation on substrate by PACD method

As can be seen from above, although the CdSe layer was successfully formed on the surface of ZnO/CdS substrate with corresponding PEC cell efficiency up to 2.88%, the deposition time of 16 h was too long for any practical processes for solar cell fabrication. Normally, a high reaction temperature would be required to overcome the activation energy in CBD methods [17, 26]. In this experiment, external light was introduced as the excitation source according to previous understanding of photochemical systems [48]. To simplify the procedure, a 405 nm semiconductor laser was applied. The surface of the sample became brown just in one minute after the reaction started, and turned black in about 1 h. As shown by figure 2, the rod diameter of the sample increased from 130 nm (before reaction, shown in figure 2(a)) to about 200 nm (after 1 h of reaction, figure 2(b)). Meanwhile, figure 2(c) demonstrates the existence of crystalline grains in the deposited materials, with a grain size of 6–10 nm and interplanar spacing of about 0.373 nm, consistent with the (100) plane of CdSe. Corresponding EDX measurement (figure 2(d)) indicated a significant existence of Se in the as-formed layer with an atomic number ratio of Se, S and Cd of 38:16:41 (details can be found in supplementary table 2S, available at stacks.iop.org/00/00/000000). Moreover, figure 2(e) shows significant diffraction peaks at 26.8° in curves I and II and 25.4° in curve II, corresponding to the (111) plane of a cubic CdS structure (JCPDS no. 21-0829) and the (111) plane of CdSe (JCPDS no. 65-2891), respectively. Apparently, CdSe has been effectively formed after 1 h of PACD treatment, which was also supported by room-temperature Raman spectroscopy in figure 2(f). For ZnO/CdS nanorods (curve I), an intensive peak at 308.8 cm^{-1} was observed, relating to the characteristic peak to the 1LO mode of CdS. After the PACD process (curve II), a peak at 203.3 cm^{-1} appeared, which belongs to the 1LO mode of CdSe.

Furthermore, the optical properties were measured by UV/vis/NIR spectroscopy before and after the reaction. As presented in figure 2(g), ZnO/CdS nanorods arrays (Spectrum I) show an absorption edge at 520 nm due to the small bandgap of CdS (2.38 eV). A significant redshift of the absorption edge to 730 nm (1.70 eV) can be observed after the CdSe PACD process (spectrum II). Apparently, the range of light absorption of the as-prepared ZnO/CdS/CdSe nanorods arrays was broadened to almost the entire spectrum of visible light. The as-fabricated nanorod arrays were also installed into a sandwich-type PEC solar cell with the *J*–*V* curves of the cells shown in figure 1(h). Consequently, the solar cells based on PACD-deposited CdSe yielded a η of 1.95% (with $J_{SC} = 9.34$ mA cm^{-2}, $V_{OC} = 0.557$ V, and FF = 0.37), which is 207% higher than the value ($\eta = 0.94\%$, $J_{SC} = 4.73$ mA cm^{-2}, $V_{OC} = 0.524$ V, and FF = 0.38) of the cell based on ZnO/CdS nanorods arrays (curve I) but lower than the optimum 2.88% result of the control samples. Nevertheless, the significantly enhanced light absorption for the CdSe sample by PACD has indicated a potential probability to improve the PEC performance by factor controls (which is also supported by the EQE measurements in figure 3S in the supplementary information).

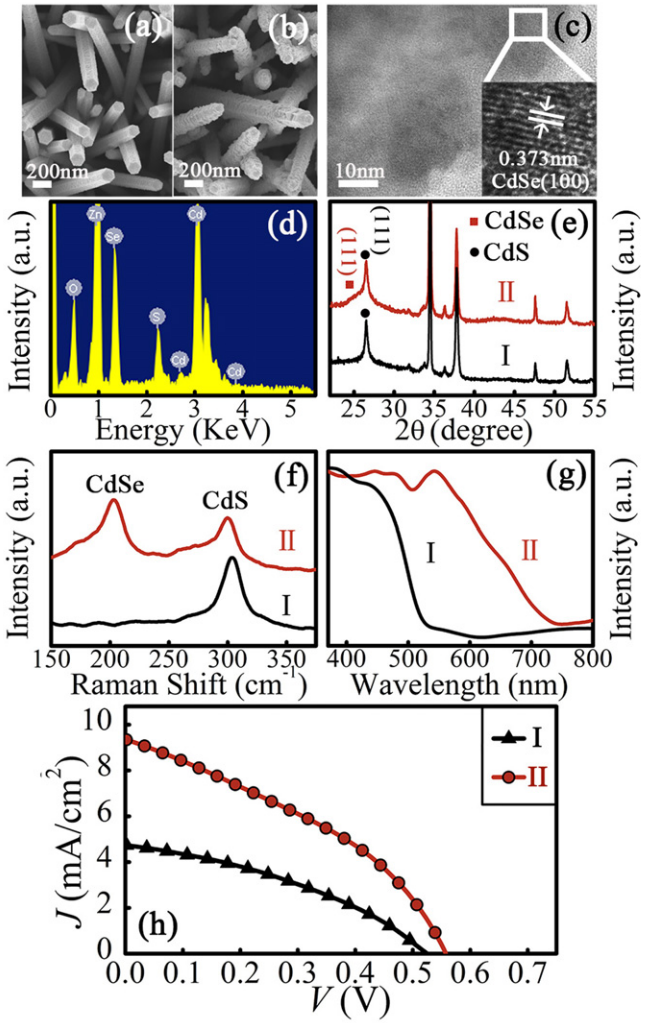

Figure 2. PACD of CdSe on ZnO/CdS nanorods substrates and the corresponding cell performance: (a),(b) top-view SEM images of the sample: (a) before and (b) after 1 h deposition; (c) TEM image the deposited sample; (d) EDX of the deposited sample; (e)–(i) results of (e) XRD, (f) Raman, (g) diffused reflectance spectra (DRS), and (h) *J*–*V* characteristics of PEC solar cells based on (I) not deposited and (II) deposited sample after 1 h deposition.

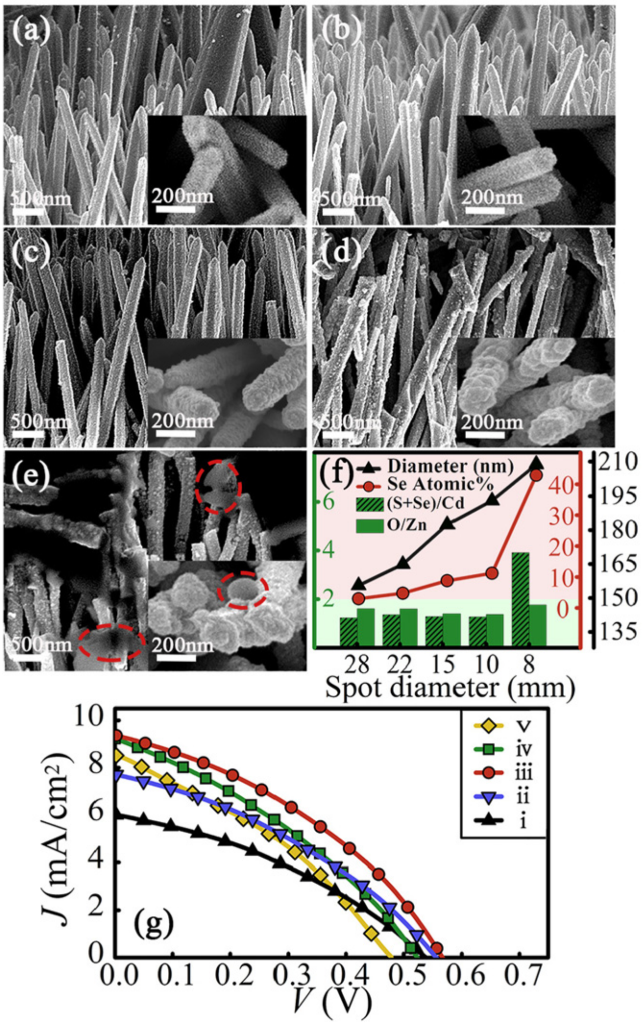

Figure 3. Influence of light power density on the CdSe formation under 50 mW 405 nm laser illumination for 1 h: (a)–(e) cross-section and top-view SEM images of ZnO/CdS/CdSe by tuning the diameter of the laser beam: (a) $D = 28$ mm, (b) $D = 22$ mm, (c) $D = 15$ mm, (d) $D = 10$ mm and (e) $D = 8$ mm; (f) average diameter, Se content, ratio of atomic content (O/Zn, (S + Se)/Cd) versus spot diameter, measured by EDX; (g) *J*–*V* characteristics of PEC solar cells with different spot diameters ((i) 28 mm, (ii) 22 mm, (iii) 15 mm, (iv) 10 mm and (v) 8 mm).

3.3. CdSe formation under varied power density of light

To study the influence of light parameters on the CdSe formation, the power density of light was varied by adjusting the diameter of the light spot optically with fixed wavelength (405 nm) and total power (50 mW). The spot diameter D was tuned to 28, 22, 15, 10 and 8 mm by a lens system with fixed deposition time of 1 h. As shown in figures 3(a)–(e), the surface of the nanorods became rougher and their diameter gradually increased with decreasing D (which means increasing power density of light). At the highest power density ($D = 8$ mm), certain big islands appeared even outside of the nanorods, as indicated by the red circle in figure 3(e). Meanwhile, figure 3(f) indicates that the average nanorod diameter gradually increased from 155 to 210 nm as the power density increased. Furthermore, the content of Se atoms increased with the increasing power density of light while the atomic ratio of (Se + S)/Cd remained at ~1.28, as shown by the EDX measurement in figure 3(f) (EDX original data can be found in supplementary table 3S). In particular, when the spot diameter was 8 mm, a drastic increase of Se content appeared, as well as (S + Se)/Cd. Subsequently, the samples were also integrated into PEC solar cells and characterized by *J*–*V* measurement, with the results demonstrated in figure 3(g). The J_{SC} and V_{OC} first increased with decreasing spot size and then began to decrease when D became less than 15 mm. When $D = 15$ mm, the cell performance reached its maximum, with $\eta = 1.96\%$, $J_{SC} = 9.36\ \mathrm{mA\ cm^{-2}}$, $V_{OC} = 0.572$ V and FF = 0.37. The corresponding power density of the light was about 60 mW cm^{-2}, which can be the threshold for further optimization.

3.4. Influence of wavelength on CdSe formation

Besides the power density, the photon energy is also an important parameter of the incident light source. Hence, PACD experiments with varied wavelength (or photon energy) were performed for the CdSe formation with fixed power density ($D = 15$ mm, laser power 50 mW) and deposition time of 1 h. Five wavelengths were chosen: 780, 650, 532, 450 and 405 nm. Significant morphological changes have taken place as the wavelength decreased (figures 4(a)–(e)). When $\lambda = 780$ nm and 650 nm (figures 4(a) and (b)), no obvious surface changes were observed. When $\lambda = 532$ nm (figure 4(c)), small particles emerged at the surface. The particles grew and clustered to larger islands on the surface as the wavelength decreased to 450 nm (figure 4(d)) and 405 nm (figure 4(e)). Meanwhile, the corresponding average diameter of each sample increased from 145 to 195 nm, as shown in the figure 4(e). Elemental analysis by EDX in figure 4(f) further configured the change in the substrate surface (EDX original data can be found in supplementary table 5S). At a laser wavelength of 780 nm, no detectable Se content can be found. From 650 nm, the amount of the Se component increased monotonically with decreasing λ. Like the previous experiment, the value of (S + Se)/Cd was also nearly a constant for $405\ \mathrm{nm} < \lambda < 650\ \mathrm{nm}$, indicating a stable growth of CdSe on the original CdS surface.

Furthermore, *J*–*V* characteristics and EQE of the PEC solar cells were also measured to study the performance of corresponding samples. As shown in figure 4(g), J_{SC} increased from 4.75 mA cm^{-2} to 9.25 mA cm^{-2} when λ decreased from 780 nm to 405 nm (details can be found in supplementary table 6S in the supporting information). Meanwhile, V_{OC} and FF gradually increased from 0.507 V to 0.570 V and from 0.30 to 0.39, respectively. Generally, the samples exhibited highest η of 2.03% when $\lambda = 405$ nm, $V_{OC} = 0.570$ V, $J_{SC} = 9.25\ \mathrm{mA\ cm^{-2}}$ and FF = 0.39. These results suggest the increasing deposition of CdSe with increasing photon energy can strongly improve the cell performance.

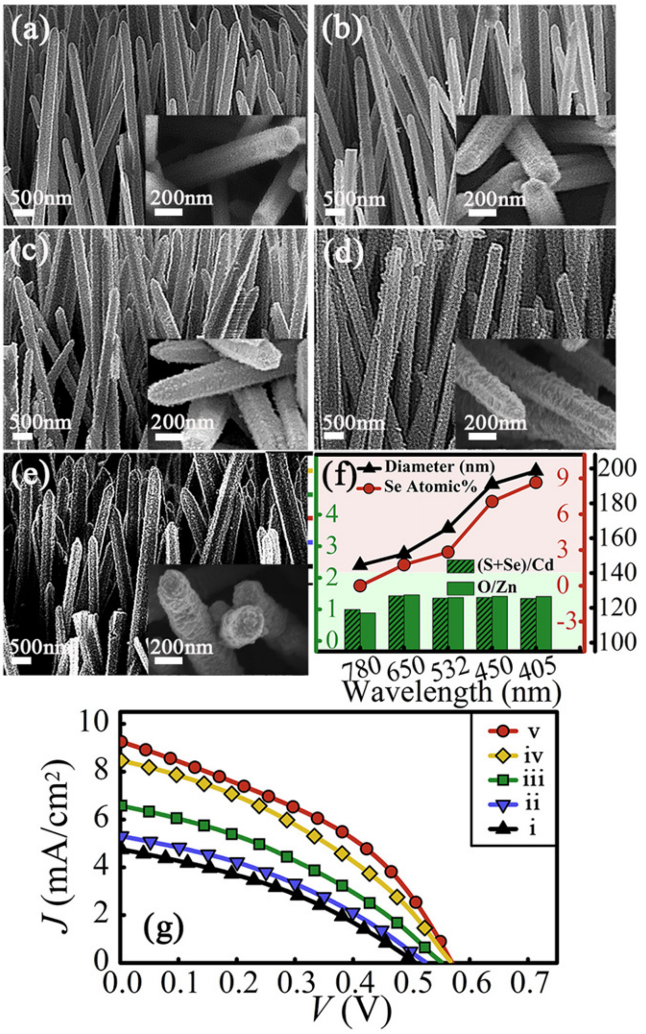

Figure 4. Influence of different photon energies on the PACD of CdSe under 50 mW laser illumination (with fixed 15 mm spot diameter) for 1 h: (a)–(e) cross-section and top-view SEM images of ZnO/CdS/CdSe with the laser wavelength from 780 nm to 405 nm: (a) 780 nm, (b) 650 nm, (c) 532 nm, (d) 450 nm, (e) 405 nm; (f) average diameter, Se content, ratio of atomic content (O/Zn, (S + Se)/Cd) versus wavelength, measured by EDX; (g) *J*–*V* characteristics of PEC solar cells under different wavelengths ((i) 780 nm, (ii) 650 nm, (iii) 532 nm, (iv) 450 nm and (v) 405 nm).

3.5. Time evolution of CdSe deposition in PACD process

As indicated by the above experiments, the number and energy of the incident photons are two key factors that significantly influence the morphology, structure and chemical composition of the as-formed materials. Yet the time evolution of the sample during such PACD process on the nanorods is still not known. Therefore, we continued to perform the experiment of PACD of CdSe with different times. According to the optimum conditions investigated previously, a 405 nm laser (50 mW) was applied with $D = 15$ mm. The time points were set at 3, 5, 10, 20, 40, 60, 120 and 180 min, as shown in figures 5(a)–(h), respectively. As the time increased, the average diameter of the rods increased from 100 to 205 nm (figure 5(i)). Meanwhile small particles developed on top of the nanorods from early stage of the reaction (figure 5(a), $t = 3$ min). As the deposition continues, as shown in figures 5(b)–(f), more and more particles began to appear at the lower parts of the rods until the whole rod was covered when $t = 120$ min (figure 5(g)). Meanwhile, some big islands emerged on the nanorods' surfaces when the deposition time was increased to 180 min (figure 5(h)). Moreover, as shown in figures 5(i) and (j), the Se content increased monotonically with increasing deposition time and the atomic ratio of (Se + S)/Cd and O/Zn remained almost constant (original data can be found in supplementary table 7S), which indicates that CdSe was stably deposited and then covered the surface of original ZnO/CdS nanorods.

Eventually, the samples with $t \geqslant 20$ min were selected and integrated into PEC solar cells to characterize their optoelectronic properties. As shown in figure 5(k), the cell efficiency increased with $t \leqslant 120$ min and then started to decrease when the growth continued. The cells yielded a highest efficiency $\eta = 3.11\%$ when $t = 120$ min, with $V_{OC} = 0.578$ V, $J_{SC} = 12.43$ mA cm^{-2} and FF = 0.43. Furthermore, the J_{SC} and V_{OC} simultaneously increased when deposition time increased from 20 min to 120 min and decreased afterwards.

3.6. Growth of material using composite light

Previous experiments have shown that significant CdSe deposition takes place for wavelengths below 532 nm and can also be enhanced by intermediate illumination intensity. Based on that, for more applicable purposes, we introduced an AM 1.5 light source into the system with a final incident light intensity reduced to 60 mW cm^{-2}, similar to the optimum intensity in the experiment in section 3.3. As shown by figure 6(a), certain cracks appeared on the surface of the as-formed materials. This phenomenon can possibly be ascribed to destruction of ZnO in similar solution by the UV component in the AM 1.5, according to related research by other groups [49, 50]. To verify this, an experiment was carried on under illumination of a high pressure Hg lamp ($\lambda \sim 365$ nm), also with a light intensity of 60 mW cm^{-2}. As shown in figure 6(b), strong destruction of the core area of the rod arrays emerged after 1 h of experiment. It also implied high energy photons (with energy higher than the bandgap of ZnO) can deteriorate the final complex structure. Moreover, the wavelength experiment has already shown that infrared radiation did not significantly contribute to the CdSe production (in the illumination level of this experiment). Therefore we considered the application of a UV/IR blocker filter (400 nm $< \lambda <$ 720 nm) to the AM 1.5 light source. As a result, no more structural damage appeared in the as-formed structure in figure 6(c). The optimized results for those experiments were achieved in 1, 1 and 1.5 h, respectively. The *J*–*V* characteristics shown in figure 6(d) demonstrate that the efficiency of the PEC cell can eventually reach 3.59% (with a $J_{SC} = 13.99$ mA cm^{-2}, $V_{OC} = 0.602$ V and FF = 42%) when fabricated by a filtered AM1.5 light source, which also suggests an applicable method simply using natural light.

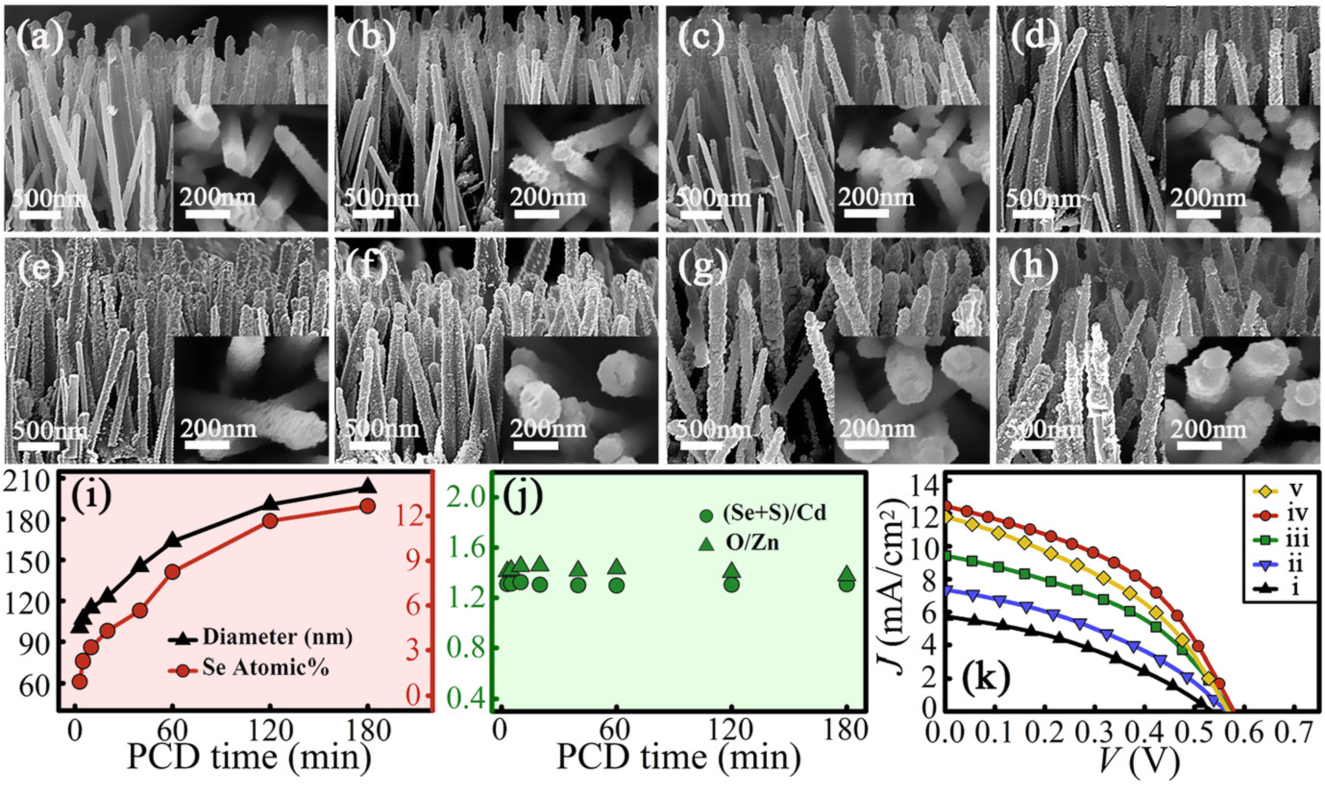

Figure 5. Influence of different deposition times on the PACD of CdSe under 405 nm 50 mW laser illumination (with fixed 15 mm spot diameter): (a)–(h) cross-section and top-view SEM images of ZnO/CdS/CdSe with deposition time from 3 min to 180 min: (a) 3 min, (b) 5 min, (c) 10 min, (d) 20 min, (e) 40 min, (f) 60 min, (g) 120 min, (h) 180 min; (i),(j) average diameter, Se content, ratio of atomic content (O/Zn, (S + Se)/Cd) versus deposition time, measured by EDX; (k) *J–V* characteristics of PEC solar cells with different deposition times ((i) 20 min , (ii) 40 min, (iii) 60 min, (iv) 120 min and (v) 180 min).

4. Discussion

The series of experiments carried out previously have revealed a significant influence of incident light on the formation of CdSe on the ZnO/CdS substrates. To understand these phenomena and investigate their further development, we hereby carried out a mechanism discussion based on the following model according to the results and normal understanding of photochemical processes [32, 51–53]:

$$\mathrm{Cd(NTA)_2^{4-}} \leftrightarrow \mathrm{Cd^{2+}} + 2\mathrm{NTA^{3-}} \tag{1}$$

$$\mathrm{ZnO/CdS} + h\nu \rightarrow \mathrm{ZnO/CdS}(e_{\mathrm{CB}}^- + h_{\mathrm{VB}}^+) \tag{2}$$

$$\mathrm{SeSO_3^{2-}} + 2e_{\mathrm{CB}}^- \rightarrow \mathrm{Se^{2-}} + \mathrm{SO_3^{2-}} \tag{3}$$

$$\mathrm{SO_3^{2-}} + 2h_{\mathrm{VB}}^+ + \mathrm{H_2O} \rightarrow \mathrm{SO_4^{2-}} + 2\mathrm{H^+} \tag{4}$$

$$2\mathrm{SO_3^{2-}} + 2h_{\mathrm{VB}}^+ \rightarrow \mathrm{S_2O_6^{2-}} \tag{5}$$

$$\mathrm{Cd^{2+}} + \mathrm{Se^{2-}} \rightarrow \mathrm{CdSe} \tag{6}$$

where e_{CB}^- and h_{VB}^+ are electrons and holes generated by the incident light, respectively. The formation of CdSe on the substrate can be generally described by three main stages (shown in figure 6(f)). At first, Cd^{2+} ions were released from complex ions of $Cd(NTA)_2^{4-}$ (equation (1)), which have been preliminarily formed by mixing $Cd(CH_3OO)_2$ with $N(CH_2COONa)_3$. They were then adsorbed onto the substrate surface. Secondly, with the illumination of light (when $h\nu > 2.38$ eV), electrons and holes can be generated from CdS substrate. The photo-excited electrons can greatly enhance the generation of Se^{2-} from $SeSO_3^{2-}$ (equations (2) and (3)). At the same time, the holes can be consumed by reactions with SO_3^{2-} in several possible routes (equations (4) and (5)). Additionally, once CdSe is formed, electrons can also be excited from CdSe and accelerate the release of Se^{2-}. Finally, adsorbed Cd^{2+} and Se^{2-} ions react immediately and form CdSe on the substrate (equation (6)). In this model, the key step is the photogeneration of electrons and holes from the semiconductor substrates. As shown in the schematic diagram in the inset of figure 6(f), the ZnO/CdS has type-II structure, which can efficiently separate electron–hole pairs and reduce their recombination. When the wavelength of incident light is lower than the absorption edge, photogenerated electrons will be injected from the CB (conduction band) of photo-excited CdS into the CB of ZnO, leading to separation of electron–hole pairs and the accumulation of electrons in the CB of ZnO. Meanwhile, the holes generated on the VB (valence band) will also accumulate due to the VB of CdS becoming more cathodic than ZnO. The separated electrons and holes will subsequently participate in the oxidation and reduction reactions.

Therefore, when the intensity of the illumination becomes higher at fixed wavelength, the increase of CdSe coverage and thickness are related to the increase of reactive

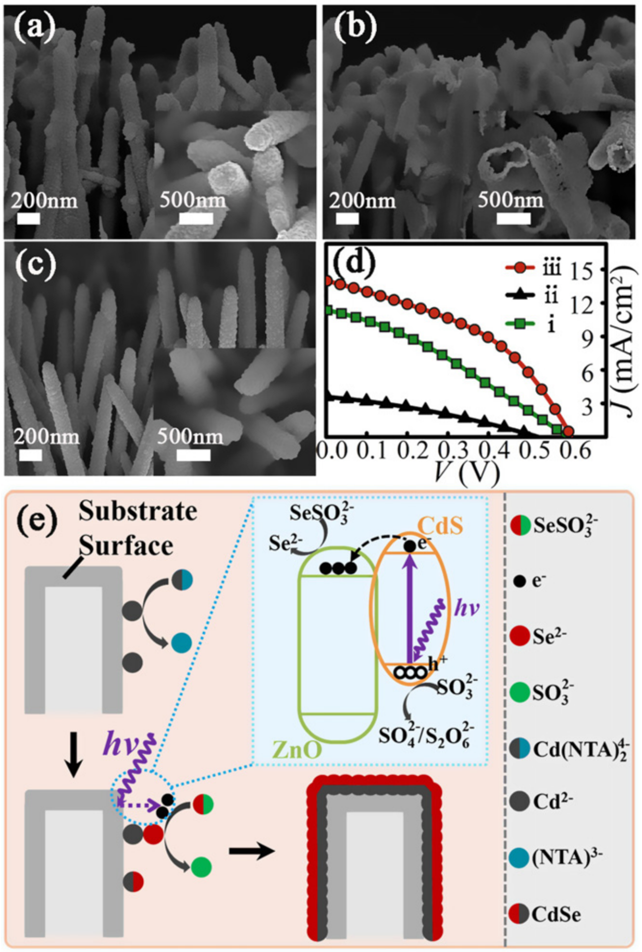

Figure 6. Influence of the mixed light source on the formation of CdSe. (a)–(c) cross-section and top-view SEM images of ZnO/CdS/CdSe with different mixed light sources: (a) 60 mW cm^{-2} of AM 1.5 for 1 h; (b) 60 mW cm^{-2} high pressure mercury lamp for 1 h; (c) 60 mW cm^{-2} AM 1.5 with a UV/IR blocker filter (400 nm $< \lambda <$ 720 nm) for 1.5 h. Corresponding (d) J–V characteristics of PEC solar cells ((i), (ii) and (iii) stands for (a), (b) and (c), respectively). (e) Schematic diagram of CdSe layer fabrication process on the substrates.

Cd^{2+} and Se^{2-} by enhanced photo-excited electrons from the substrate. With the band alignment of CdSe and CdS [54], increasing the thickness of CdSe could not only increase the absorption of light but also accelerate separation of photo-excited electron–hole pairs, which could increase J_{SC}, V_{OC} and the shunt resistance while decreasing the series resistance. However, it can also be observed in figure 3 that the sample surface was generally smooth when spot diameter was larger than 15 mm, but rather rough for the diameter less than 15 mm. The island formation could simultaneously increase the thickness of sensitizer layer and the number of defects in it, which may confine photo-excited electron-hole and recombine the photo-excited electrons [55, 56]. Hence, significant island formation may reduce J_{SC}, V_{OC} and the shunt resistance while increasing the series resistance. Therefore we finally discovered a nonmonotonic behavior versus the spot size of the cell performance. The rougher surface under stronger illumination may possibly be due to the enhanced etching effect on CdSe in the reaction system under higher light power [57]. The excessive Se formed at highest power density was likely from the same origin as in the research work from other groups on Se photodeposition in other systems [58–61]. In the study of wavelengths at fixed power, the number of photons decreased with shorter wavelength. However, the photon absorption coefficient of the substrate was also stronger for shorter wavelengths, as shown in figures 1(f), 2(g) and supplementary figure 2S. Therefore, the increase of the as-formed CdSe content in figure 4 is likely to be attributed to stronger electron excitation on the substrate induced with higher photon energy.

On the time evolution of the deposited CdSe, a possible explanation for the nonmonotonic change of its opto-electronic properties can be the intensity distribution of the incident light and the preferential growth of material against the incident direction. At early stages of the reaction, a rigid layer of CdSe particles had already formed on top of the rods while small particles had just emerged at the lower positions on the rods. As the time increased, more CdSe islands were developed to gradually form a layer at the lower position which was previously covered by discrete islands. This process may not only enhance the light absorption due to more CdSe coverage but also increase the electron transport ability, and led to higher efficiency of the solar cells before the whole rod was covered by CdSe. However, when the whole rod surface became covered by CdSe, the fabrication in the radial direction became predominant. Therefore the series resistance began to increase with the increasing average thickness due to longer transfer path for the photo-excited electrons, which in general induced lower cell efficiency.

Additionally, during the reaction process under the illumination of UV light, though the CdSe formation can be further enhanced under strong electron excitation, the ZnO structure in the substrate apparently deteriorated, as shown in figure 6. This might have been due to the photocorrosion in aqueous solution under UV irradiation, which was induced by the attacks of residual photo-generated holes with the Zn–O bond and disassociation of Zn^{2+} from ZnO surface [49, 50]. Consequently, the cell performance will be negatively influenced as ZnO is photoelectrons collection and delivering layer. When the ZnO/CdS/CdSe was integrated in PEC cells with polysulfide electrolyte, such instability can be significantly reduced due to the strong consumption of the photogenerated holes by high concentration $S^{2-}/S_n{}^{2-}$ and the blocking effect of the ZnS passive layer on direct contact of inner ZnO and electrolyte [55, 62, 63].

From above the discussions, we can conclude that intermediate wavelength with photon energy between the bandgap of CdS (2.4 eV) and ZnO (3.3 eV), appropriate light power density and reaction time would be the key factors to optimize this system. The performance of the products by the PACD method could still be improved by alternations such as further parameter tuning of the composite light source, surface modification of substrates, variation of precursors and application of other electrolyte/counter electrode systems, if considering the results of CdS/CdSe cosensitized system in previous works [26, 64, 65]. The as-fabricated CdSe may be used in photoelectrochemical hydrogen generation due to its effective light absorption and type-II graded bandgap structure. By tuning their average size, they may also be applied in quantum-dot light-emitting devices with strong electronic coupling [66]. More importantly, the same method could be easily applied for more types of QDs and thin films on other nanostructured substrates with just simple precursors. For example, $Na_2S_2SO_3$ are also photo-sensitive and can be applied in PACD method as the source of S^{2-} to fabricate sulfide QDs [3, 36].

5. Conclusion

In summary, uniform CdSe layers with variable thickness were directly formed on the substrate at room temperature with significantly enhanced light absorption and electronic property. Systematic investigations have demonstrated that the morphology and quality of as-formed CdSe QDs are significantly influenced when tuning the light parameters, which controls the releasing of Se^{2-} from Na_2SeSO_3. The study on the influence of time has indicated a top-down growth along the incident direction and possible deterioration of CdSe layer for too long growth time. The cell efficiency reached 3.59% simply with a modified natural light source and without additional physical or chemical treatment. This result is also significantly higher than the control sample fabricated under similar chemical conditions by conventional the CBD method but with growth time greatly shortened to one order of magnitude. Hopefully, further studies on mechanism and technologies may still extend the range of materials and promote controllability toward applicable solar cells and other devices.

Acknowledgments

This work was supported by the National Major Basic Research Project of 2012CB934302 and Natural Science Foundation of China under contracts 11204176, 11174202, and 61234005.

References

[1] Graetzel M, Janssen R A, Mitzi D B and Sargent E H 2012 *Nature* **488** 304–12

[2] Jeon N J, Noh J H, Yang W S, Kim Y C, Ryu S, Seo J and Seok S I 2015 *Nature* **517** 476–80

[3] Tada H, Fujishima M and Kobayashi H 2011 *Chem. Soc. Rev.* **40** 4232–43

[4] Xu J, Yang X, Yang Q D, Wong T L, Lee S T, Zhang W J and Lee C S 2012 *J. Mater. Chem.* **22** 13374–9

[5] Santra P K and Kamat P V 2012 *J. Am. Chem. Soc.* **134** 2508–11

[6] Ryu J, Lee S H, Nam D H and Park C B 2011 *Adv. Mater.* **23** 1883–8

[7] Sugaya T, Numakami O, Oshima R, Furue S, Komaki H, Amano T, Matsubara K, Okano Y and Niki S 2012 *Energ. Environ. Sci.* **5** 6233–7

[8] Xiong Y, Tao L, Liu H and Shen W Z 2013 *J. Mater. Chem.* A **1** 783–91

[9] Tao L, Xiong Y, Liu H and Shen W Z 2012 *J. Mater. Chem.* **22** 7863–70

[10] Song X H, Wang M Q, Deng J P, Yang Z, Ran C M, Zhang X Y and Yao X 2013 *ACS Appl. Mater. Interfaces* **5** 5139–48

[11] Chao X, Nie B, Zeng L and Yu S H 2014 *ACS Nano* **8** 4015–22

[12] Wang H, Wang B, Yu J, Hu Y, Xia C, Zhang J and Liu R 2015 *Sci. Rep.* **5** 9305

[13] Adhyaksa G W, Lee G I, Baek S W, Lee J Y and Kang J K 2013 *Sci. Rep.* **3** 2711

[14] Xiao M W, Wang L S, Wu Y D, Huang X J and Dang Z 2008 *Nanotechnology* **19** 015706

[15] Tao L, Xiong Y, Liu H and Shen W 2014 *Nanoscale* **6** 931–8

[16] Moloney M P, Govan J, Loudon A, Mukhina M and Gun'ko Y K 2015 Preparation of chiral quantum dots *Nat. Protocols.* **10** 558–73

[17] Pan Z and Zhang H 2012 *ACS Nano* **6** 3982–91

[18] Wang F, Dong H, Pan J, Li J, Li Q and Xu D 2014 *J. Phys. Chem.* C **118** 19589–98

[19] Sheng P, Li W, Cai J, Wang X, Tong X, Cai Q and Grimes C A 2013 *J. Mater. Chem.* A **1** 7806–15

[20] Chou T P, Zhang Q, Fryxell G E and Cao G Z 2007 *Adv. Mater.* **19** 2588–92

[21] Zhang Q, Dandeneau C S, Zhou X and Cao G 2009 *Adv. Mater.* **21** 40871–08

[22] Zhang Q, Yodyingyong S, Xi J, Myers D and Cao G 2012 *Nanoscale* **4** 1436–45

[23] Tian J, Uchaker E, Zhang Q and Cao G 2014 *ACS Appl. Mater. Interfaces* **6** 4466–72

[24] Li C, Yang L, Xiao J, Wu Y C, Sondergaard M, Luo Y, Li D, Meng Q and Iversen B B 2013 *Phys. Chem. Chem. Phys.* **15** 8710–5

[25] Xu J, Chen Z and Zhang W 2014 *Adv. Mater.* **26** 5337–67

[26] Choi Y, Seol M, Kim W and Yong K 2014 *J. Phys. Chem.* C **118** 5664–70

[27] Gimenez S, Lana-Villarreal T, Gomez R, Agouram S, Munoz-Sanjose V and Mora-Sero I 2010 *J. Appl. Phys.* **108** 064310

[28] Yu X Y, Lei B X, Kuang D B and Su C Y 2011 *Chem. Sci.* **2** 1396–400

[29] Zhao W B, Zhu J J and Chen H Y 2003 *J. Cryst. Growth* **252** 587–92

[30] Preetha K C and Remadevi T L 2014 *J. Mater. Sci: Mater. Electron* **25** 1783–91

[31] Justin Raj C, Karthick S N, Park S, Hemalatha K V, Kim S K, Prabakar K and Kim H J 2014 *J. Power Sources* **248** 439–46

[32] Tian J, Zhang Q, Uchaker E, Liang Z, Gao R, Qu X, Zhang S and Cao G 2013 *J. Mater. Chem.* A **1** 6770–5

[33] Becker M A, Radich J G, Bunker B A and Kamat P V 2014 *J. Phys. Chem. Lett.* **5** 1575–82

[34] Sauvage F, Davoisne C, Philippe L and Elias J 2012 *Nanotechnology* **23** 395401

[35] Zhao W B, Zhu J J and Chen H Y 2004 *Scr. Mater.* **50** 1169–73

[36] Ichimura M, Goto F and Araib E 1999 *J. Electrochem. Soc.* **146** 1028–34

[37] Steinmiller E M P and Choi K-S 2009 *Proc. Natl Acad. Sci. USA* **106** 20633–6

[38] Liu Y, Sun L, Wu J, Fang T, Cai R and Wei A 2015 *Mater. Sci. Eng.* B **194** 9–13

[39] Sun Z H, Liu Z K, Li J H, Tai G A, Lau S P and Yan F 2012 *Adv. Mater.* **24** 5878–83

[40] Zhang Q X, Chen G P, Yang Y Y, Shen X, Zhang Y D, Li C H, Yu R C, Luo Y H, Li D M and Meng Q B 2012 *Phys. Chem. Chem. Phys.* **14** 6479–86

[41] Zhang H, Quan X, Chen S, Yu H and Ma N 2009 *Chem. Mater.* **21** 3090–5

[42] Zhong D K, Cornuz M, Sivula K, Graetzel M and Gamelin D R 2011 *Energ. Environ. Sci.* **4** 1759–64
[43] Janáky C, de Tacconi N R, Chanmanee W and Rajeshwar K 2012 *J. Phys. Chem.* C **116** 19145–55
[44] Lu Z *et al* 2012 *J. Phys. Chem.* C **116** 2656–61
[45] Phuruangrat A, Thongtem T and Thongtem S 2009 *Mater. Lett.* **63** 1538–41
[46] Comas F, Trallero-Giner C, Studart N and Marques G E 2002 *Phys. Rev.* B **65** 073303
[47] Nien Y T, Zaman B, Ouyang J, Chen I G, Hwang C S and Yu K 2008 *Mater. Lett.* **62** 4522–4
[48] Wardle B 2009 *Principles and Applications of Photochemistry* (Hoboken, NJ: Wiley) pp 197–212
[49] Zhang L, Cheng H, Zong R and Zhu Y 2009 *J. Phys. Chem.* C **113** 2368–74
[50] Han J, Qiu W and Gao W 2010 *J. Hazard. Mater.* **178** 115–22
[51] Park H, Kim Y K and Choi W 2011 *J. Phys. Chem.* C **115** 6141–8
[52] Zhao H, Dong Y, Jiang P, Wang G, Miao H, Wu R, Kong L, Zhang J and Zhang C 2015 *Chem. and Eng.* **3** 969–77
[53] Irshad A and Munichandraiah N 2015 *J. Electrochem. Soc.* **162** H235–43
[54] Lee Y-L and Lo Y-S 2009 *Adv. Funct. Mater.* **19** 604–9
[55] Yin X, Que W, Fei D, Xie H, He Z and Wang G 2013 *Electrochim. Acta* **89** 561–70
[56] Pedro V G and Xu X 2010 *ACS Nano* **4** 5783–90
[57] Lim S J, Kim W and Shin S K 2012 *J. Am. Chem. Soc.* **134** 7576–9
[58] Perakh M, Peled A and Feit Z 1978 *Thin Solid Films* **50** 273–82
[59] Perakh M and Peled A 1978 *Thin Solid Films* **50** 283–91
[60] Perakh M and Peled A 1978 *Thin Solid Films* **50** 293–300
[61] Sadtler B, Burgos S P, Batara N A, Beardslee J A, Atwater H A and Lewis N S 2013 *Proc. Natl Acad. Sci. USA* **110** 19707–12
[62] Seol M, Ramasamy E, Lee J and Yong K 2011 *J. Phys. Chem.* C **115** 22018–24
[63] Kim H, Hwang I and Yong K 2014 *ACS Appl. Mater. Interfaces* **6** 11245–53
[64] Kim H and Yong K 2013 *Phys. Chem. Chem. Phys.* **15** 2109–16
[65] Zhu Z, Qiu J, Yan K and Yang S 2013 *ACS Appl. Mater. Interfaces* **5** 4000–5
[66] Mashford B S *et al* 2013 *Nat. Photonics* **7** 407–12